Can Electron Transport through a Blue-Copper Azurin Be Coherent? An Ab Initio Study

Carlos Romero-Muñiz,[∇] María Ortega,[∇] J. G. Vilhena, Ismael Díez-Pérez, Rubén Pérez, Juan Carlos Cuevas,* and Linda A. Zotti*

ACCESS | Metrics & More | Article Recommendations | Supporting Information

ABSTRACT: Multiple experiments on the electron transport through solid-state junctions based on different proteins have suggested that the dominant transport mechanism is quantum tunneling (or coherent transport). This is extremely surprising given the length of these molecules (2−7 nm) and their electronic structure (mainly comprising very localized molecular orbitals). Overall, this is probably the single most important puzzle in the field of biomolecular electronics and calls for rigorous calculations of the tunneling probability in protein-based junctions. Motivated by these experiments, we tackle here this problem and report a comprehensive theoretical study of the coherent electron transport in metal−protein−metal junctions based on the blue-copper azurin from *Pseudomonas aeruginosa*, which is the workhorse in protein electronics. More precisely, we focus on single-molecule junctions realized in STM-based experiments and analyze a wide variety of contact scenarios. Our calculations are based on a combination of molecular dynamics simulations and ab initio transport calculations. Our results unambiguously show that when azurin is not deformed and retains its pristine structure, the end-to-end tunneling probability is exceedingly small and does not give rise to any measurable electrical current. On the other hand, we find that much higher tunneling probabilities are possible when either the STM tip (indented from the top) substantially compresses the protein or the protein is contacted sideways, significantly reducing the effective junction length. We also show that in certain configurations, the presence of surrounding water can also increase the conductance but it cannot explain the high conductance values reported experimentally. In all cases, the current is found to flow through the Cu atom of this metalloprotein, although the role of several other levels close to the Fermi energy cannot be ruled out. We remark that we only evaluate the efficiency of coherent transport and the analysis of the relevance of other potential charge-transport mechanisms is out of the scope of our work.
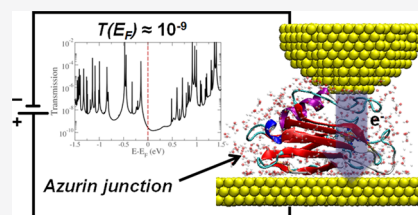
INTRODUCTION

The advance in experimental techniques, which enable the fabrication of metal−protein−metal junctions, has opened up new avenues in the field of nanotechnology.[1] Proteins present unique properties in terms of chemical recognition, self-assembly, and optoelectronics.[2,3] Thus, the foreseen possibility of exploiting such properties in electrical devices such as field-effect transistors, sensors, solar cells, and biocompatible flexible implants has attracted enormous interest and prompted numerous studies.[4−8] By now, the electron transport through proteins incorporated in solid-state junctions has been widely explored using a variety of experimental techniques. For instance, protein monolayers have been investigated with Si platforms,[9,10] suspended-wire techniques,[11−13] or employing EGaIn top electrodes.[14,15] These techniques have the advantage of producing very stable contacts that enable temperature-dependent measurements that are important for elucidating the transport mechanism. Electron transport through individual proteins (or at least a small number of them) has also become possible, thanks to the use of scanning tunneling microscopy (STM)[16−18] and conductive-probe atomic force microscopy (CP-AFM).[8,19−22] Many experiments

have been carried out with these techniques to study different proteins and reported temperature-independent electron transport,[10,13,14,21,23−27] which has been interpreted as evidence that (coherent) tunneling is the dominant transport mechanism in these junctions. This is certainly striking taking into account the size of these molecules (2−7 nm) and their chemical composition (with amino acid residues that are poorly conductive). In principle, tunneling is not the only mechanism that can lead to a temperature-independent electron transport. For instance, hopping conduction can also be temperature-independent but it requires very special conditions such as on-resonant transport and very low activation energies.[28,29] Moreover, tunneling is the only mechanism that can consistently explain other important facts such as the observation of (i) inelastic electron
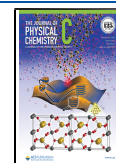
tunneling,[11,27] (ii) resonant-like behavior,[27] or (iii) temperature-independent electron transport all the way to 4 K.[21] So, it is difficult to ignore the overwhelming evidence in favor of tunneling in these junctions but its occurrence continues to be extremely puzzling and, currently, the issue on how it is possible at all to have quantum tunneling through individual proteins is one of the most pressing open questions for the theory in the field of biomolecular electronics.

This problem is very difficult to tackle due to, among other things, the large size of proteins (with thousands of atoms), the variety of possibilities to contact a protein,[2] and the crucial role played by fluctuations,[30] either thermal or induced by the presence of a solvent. Despite the enormous progress made in modeling tunneling events within proteins,[31,32] the same does not apply to the computational description of electron tunneling in metal−protein−metal junctions. Indeed, the issues listed above have thus far hindered the use of the standard ab initio transport approaches, mainly based on density functional theory (DFT), that are regularly employed to describe the coherent transport in molecular junctions made of small organic molecules.[33] In fact, the theoretical study of electron transport in protein junctions has been mainly carried out with the help of simple phenomenological models, often borrowed from the field of electron transfer;[34,35] see, e.g., ref 29 and references therein. Fortunately, the recent progress in large-scale DFT calculations has paved the way for the analysis of the electronic structure of entire proteins[36] and protein-based molecular junctions.[13,37] In this work, we extend those ab initio approaches to describe the coherent transport through single-protein junctions. To be precise, we focus on the case of azurin from *Pseudomonas aeruginosa* whose electron transport properties have been studied quite extensively.[2,6,9−13,16−18,21,27] This protein belongs to the class of redox metalloproteins and is crucial in the bacterial energy conversion system.[38] Consequently, their electron properties have been analyzed by numerous studies.[39−43] In particular, different experiments with azurin monolayers have shown temperature-independent electron transport,[10,11,21,27] interpreted as a sign of tunneling, and single-azurin experiments have reported remarkably high conductance values of up to 10^{-5} G_0,[16,18] where $G_0 = 2e^2/h$ is the quantum of conductance ($\sim(12.9$ k$\Omega)^{-1}$). This fact means that, if the transport was coherent, the tunneling probability would be as high as 10^{-5}, which is comparable to the values found in molecular junctions based on small organic molecules (<1 nm).[33] It is important to highlight that the electrical current measured in an STM-based single-protein junction is fundamentally different from the photoinduced experiments performed in the past,[44] where the former characterizes an actual hybrid nanobioelectronic device. In this work, we report the first electron transport calculations for azurin-based junctions based on fully ab initio calculations. To this aim, we combined molecular dynamics simulations with DFT calculations. The former was employed to obtain the geometries of the junctions, while the latter was used to compute their electronic structures. We then focused on the coherent component of the electron transport, evaluating the electrical conductance within the Landauer formalism and with the help of rigorous nonequilibrium Green's function (NEGF) techniques. Previous literature has raised concerns about the validity of this approach in the case of systems for which sequential tunneling becomes relevant.[45,46] However, the main purpose of our work is to verify whether fully coherent transport is plausible at all and thus we will adopt the Landauer

approach as it is the most suitable for such a case. Very importantly, ref 45 explained the caveats, which ensure the validity of the Landauer model by comparing the results obtained with this method with those obtained by time-dependent NEGF. There, it was shown that Landauer can be applied when (i) the fluctuations do not affect the degree of localization of the molecular orbitals responsible for transport and (ii) the tunneling time is shorter than the molecular correlation time. In our work, by focusing on coherent transport only, we have thus assumed that these conditions are met. We also note that the second requirement would probably be satisfied in experiments carried out at low temperatures like, for instance, in those reported in ref 27. Among the possible experimental scenarios, we chose to focus on single-protein junctions mimicking those obtained with STM-based techniques. In these experiments, trapping proteins between gold electrodes can be achieved by either break-junction dynamic tapping or blinking techniques.[18] In the former, the tip is brought into close proximity with the surface until the point it makes contact. Subsequent fast pulling of the tip can occasionally cause a protein (previously deposited on the surface) to bridge the tip−surface gap. In the latter instead, the tip is placed at a close distance from the protein, avoiding physical contact. However, because of its thermal fluctuations, the protein spontaneously attaches and detaches from the tip. When a chemical bond is established, jumps in the current signal are detected. This technique had already been used with various types of smaller molecules.[47−50] It was also introduced in protein-based experiments to avoid possible deformations that the abrupt and continuous indentation and fast pulling of the tip in the break-junction method might induce in the protein folding. In our study, we considered a large variety of junctions, which can be formed with these two techniques. Our results show that as long as azurin is gently contacted and its structure is not substantially altered, the tunneling probability is exceedingly small and the corresponding coherent conductance is simply not measurable. However, we also show that the coherent conductance can be greatly enhanced, and it may eventually become measurable, by indenting the STM tip from the top and partially squeezing the protein or by laterally contacting the protein with the tip, which in practice corresponds to a situation with a reduced effective length of the junction. To complete our study, we also explored the role of the water molecules surrounding the junctions in the transport properties of the different types of contact geometries.

■ METHODS

Molecular Dynamics Simulations. All of the simulations were performed using the AMBER14 software suite[51] with NVIDIA GPU acceleration.[52−54] The ff14SB force field[55] was used to describe all standard amino acids present in the azurin. The interatomic potentials of the copper atom and its corresponding five ligands were described using a quantum mechanically derived force field.[56] This force field includes both bonded and nonbonded terms between the Cu^{2+} atom and its five ligands and has been widely used to model the blue-copper azurin protein.[5,18,57−60] The X-ray crystallographic structure of azurin was obtained from the protein data bank[61] with the PDB code 4AZU.[62] Protons were added to the protein structure according to the calculated ionization states[63] of its titratable groups at a pH of 4.5, which corresponds to that used in the experiments of ref 18. The protonation state of
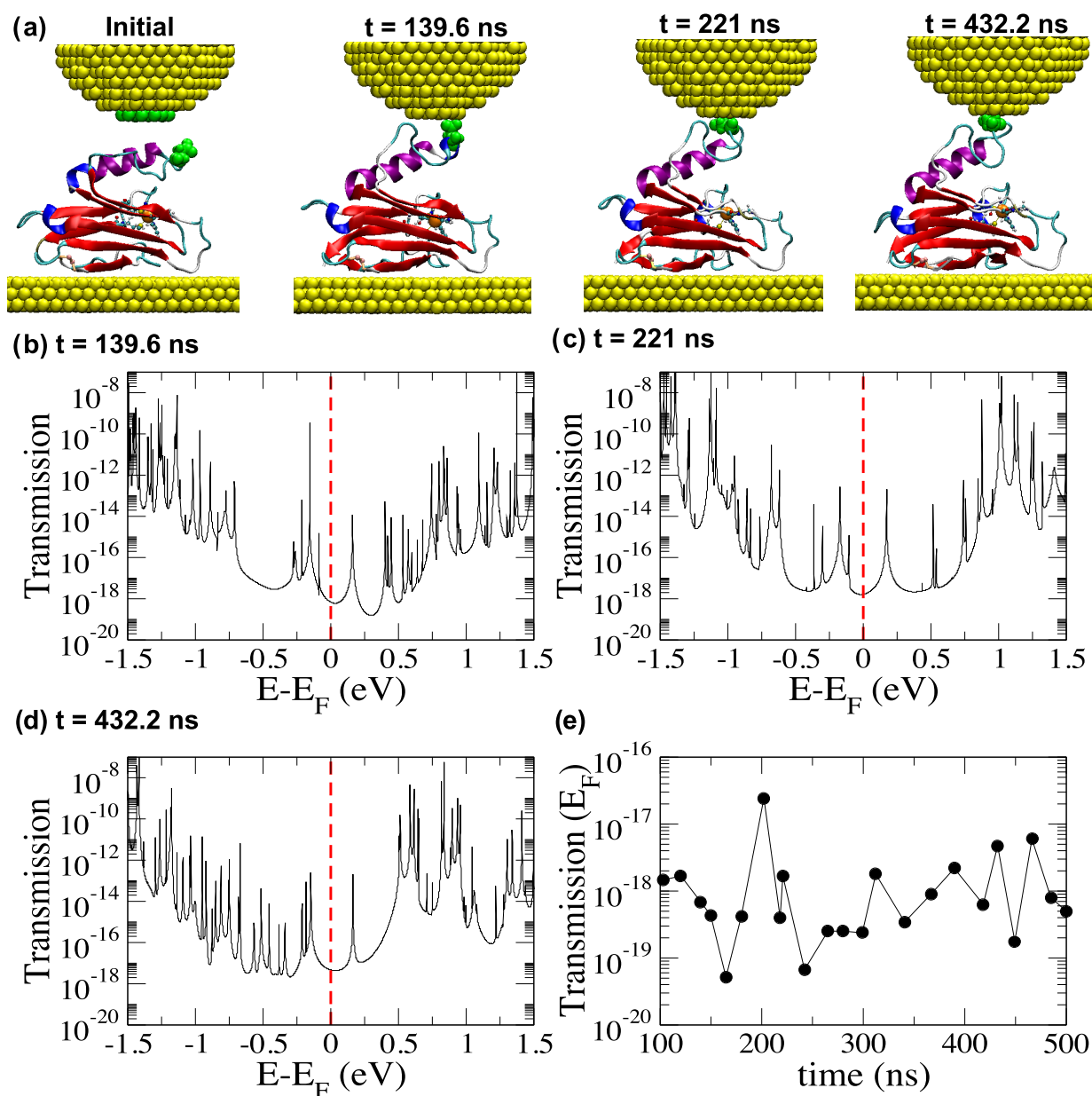
Figure 1. (a) Selected junction geometries obtained in the MD simulations of the blinking process. The leftmost geometry corresponds to the initial configuration, while the other three, indicated with the simulation time, correspond to geometries subsequent to the formation of the protein−tip bond. The aspartic acid 69 has been marked in green as one of the main anchoring groups. (b−d) Transmission as a function of energy (measured with respect to the Fermi energy E_F) for three of the geometries shown in panel (a). As a guide to the eye, the red vertical lines indicate the position of the Fermi level. (e) Transmission at the Fermi energy for 23 representative geometries in the blinking process, marked with the simulation time.

the protein corresponds to a pH of 4.5. Details about this were reported in the SI of ref 36. The net charge of the resulting azurin structure was zero. In all our simulations, the gold−azurin−gold junction consisted of a Au(111) surface where the protein was initially adsorbed (see the SI and ref 37 for further details) and a Au(111) tip with a 2 nm radius that interacts with the adsorbed protein. The Au surface was modeled by an 8 × 8 nm^2 slab and was composed of three atomic layer-thick slabs. The positions of the atoms in the lowest layer were fixed during the MD runs with a harmonic restraint of 5 kcal/mol Å^2. In this work, we assume that the S−S bridge between C3 and C26 is not broken upon adsorption. As a result, no S−Au bonds are allowed to form between these cysteines and the surface. At this point, neither single-molecule experiments[18]

nor simulations allow us to ascertain the presence/lack of such bonds. However, considering the large energy required to enable the formation of S−Au—first, by breaking the S−S bridge and then by reorganizing the surrounding amino acids so S may approach the surface—this assumption seems a sensible one. Moreover, we have tested the influence that breaking the S−S bridge (and consequently increasing the S−Au) would have upon the adsorption and protein con-formation. The results (Figure S1) show that both the structure and adsorption configuration (including the relative distance of S−Au) are preserved regardless. The surface/tip gold atoms were described using CHARMM-METAL,[64,65] which is thermodynamically consistent with the force field used to describe the protein, and it has been successfully

employed to study similar inorganic—biomolecular interfaces.[65] Additionally, recent cryoforce spectroscopy[66] and noncontact AFM[67] experiments demonstrate the suitability of this force field to describe both the mechanical properties of Au—molecule—Au contacts as well as molecular diffusion coefficients. The junction is fully embedded in a water medium in all of the simulations. The water is described using the explicit TIP3P model.[68] We used, in all of the cases, periodic boundary conditions with a rectangular box and particle mesh Ewald to account for long-range electrostatic interactions. Van der Waals contacts were truncated at a real-space cutoff of 10 Å. SHAKE algorithm was used to constrain bonds containing hydrogen, thus allowing us to use an integration step of 2 fs. Coordinates were saved every 1000 steps. The MD protocols followed for describing the indentation and blinking scenarios were thoroughly explained in refs 18 and 37, respectively. The details about the lateral indentation MD protocol are reported in Section S2 of the Supporting Information (SI).

Density Functional Theory. We have carried out density functional theory (DFT) calculations on input geometries, which were extracted from the MD simulations described above. To this aim, we have used the OpenMX code, which is based on highly optimized numerical pseudoatomic orbitals (PAOs).[69,70] A similar approach was already used for our previous work on gas-phase azurins,[36] azurin-based junctions,[37] and cytochrome c.[13] When importing the MD geometries into the DFT calculations, the outermost layers of the tip and the surface (those that are farthest from the protein) were removed for computational reasons. As a result, the substrate included in these ab initio calculations consisted of a three-layer slab of 54.6×42.3 Å^2 and 969 atoms, while the tip consisted of 252 atoms. More details about this choice are reported in Section S5. In all cases, the water molecules surrounding the junction were initially removed. For selected structures in each of the three sets, water molecules within a distance of 3 Å from the protein were included, with the aim of investigating the role of water in the electron transport. We have used the Perdew—Burke—Ernzerhof (PBE) exchange and correlation functional[71] and norm-conserving pseudopotentials.[72] Single-ζ basis sets were used for all species involved in the calculations (including the gold tip and substrate) except for the Cu center. In this latter case, a double-ζ basis set was employed. A comparison between the electronic structure obtained with this choice and with a fully double-ζ basis set for the isolated protein can be found in the SI of ref 36, showing no relevant changes, which could affect the transport properties. The cutoff radii of the PAOs were carefully selected, namely, 8 Bohr (Cu), 7 Bohr (S), and 5 Bohr (C, N, O, and H). As the cutoff radius of the basis set can be crucial in the tunneling regime,[73] a compromise between computational cost and accuracy was achieved by using a cutoff radius of 7 Bohr for the Au atoms belonging to the regions of the tip and the substrate farthest from the protein, while a cutoff of 9 Bohr was adopted for the atoms closest to it. Increasing the cutoff radii of the other species is not expected to affect the conductance significantly, as a comparison between the spatial localization of the frontier orbitals with cutoff radii of 5 and 7 Bohr only showed minimal changes. The electronic self-consistency is achieved by a Pulay mixing scheme based on the residual minimization method in the direct inversion iterative subspace (RMM-DIIS)[74] with a Kerker metric,[75] using an energy cutoff of 10^{-8} Ha as a convergence criterion. More details about the strategies adopted to achieve the self-

consistent-cycle convergence can be found in refs 36 and 37. The zero-bias transmission as a function of energy was finally computed in the spirit of the Landauer formalism and making use of NEGF techniques (see Section S1 in the SI for further details).

■ RESULTS AND DISCUSSION

Molecular Dynamics Simulations. We have carried out molecular dynamics simulations (MD) to obtain a large set of geometrical structures of gold—azurin—gold junctions, which are likely to be formed in STM-based experiments. The complexity of the processes occurring in the aforementioned experiments prevents us from describing them in full detail since our simulations are very computationally demanding. We have, therefore, focused on three possible scenarios, which will be henceforth referred to as blinking, top indentation, and lateral indentation, respectively, which globally embrace a wide variety of key plausible structures. The blinking simulation (Figure 1a) describes quite well the junction formation taking place during an experiment based on the blinking technique described above. All of the details about this simulation have already been thoroughly described in ref 37, and the junction evolution can be summarized as follows: while the tip is kept at a fixed distance from the surface and the β-barrel of the protein lies flat on the surface, the α-helix is initially involved in an up/down motion. This leads it to bind to the gold tip initially via residue 76 only and, in a later stage, via both residues 76 and 69. The end of the blinking event (corresponding to the current drop) is not described for the reasons explained above. In the indentation simulation, instead, a tip is brought close to the protein from above in a stepwise manner until contact is formed (Figure 2a).[18] The tip movement in this case resembles that occurring during a break-junction experiment. However, as our simulations are very computationally demanding, we do not describe the tip crashing on the surface and its subsequent fast pulling but instead limit our study to a simplified case as that described above. Finally, the lateral indentation refers to a tip approaching the protein sideways (Figure 3a). The resulting structures could actually correspond to some of those formed in the experiments within both blinking and break-junction techniques. In this type of simulation, binding to the tip takes place through two well-differentiated azurin regions, i.e., the α-helix arm and the azurin hydrophobic patch,[5] D69, L68, A65, G67, and N42 being the amino acids involved in the anchoring (see the SI for further details). The structures ensuing from the lateral indentation are clearly different from the other two cases because of the shorter tip—surface distance and the different geometrical surface—protein—tip alignment. Even though they are the ones that better simultaneously preserve the azurin tertiary and secondary structures (see the SI for further details). As for the indentation and blinking, although one might naively expect their respective final geometries being very similar, there is a main difference between the two sets: it lies in the kinds of deformations induced in the protein tertiary and secondary structures.[18,37] In the indentation, the impact of the tip can cause a slight compression of the protein although it was shown[18] that the folding/secondary structure is preserved up to a distance of 2.5 Å from the surface (see the α-helix content evolution in Figure S4). Conversely, in the blinking technique, the spontaneous attachment does not substantially change the protein secondary structure (see Figure S4) but can cause a separation between the α-helix and the β-barrel (as shown in
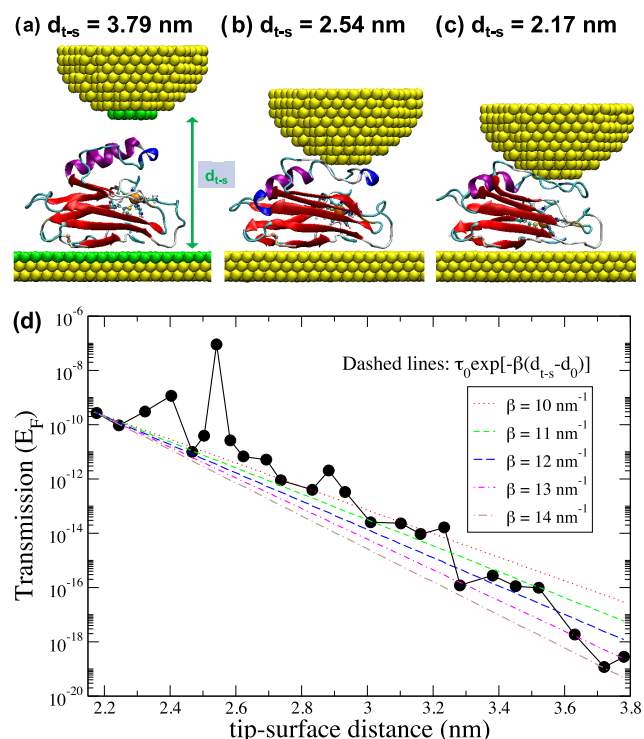
Figure 2. (a−c) Three of the junction geometries obtained during the simulations of an STM tip indentation. They are labeled according to the tip−surface distances (d_{t-s}). d_{t-s} is defined as the difference between the z coordinate of the bottom-most tip layer geometric center and the uppermost surface layer geometric center (see the schematic representation in panel (a)). (d) Transmission at the Fermi energy as a function of the tip−sample distance (filled circles) for a series of geometries obtained in the simulations of the tip indentation. The different dashed lines correspond to an exponential decay, as indicated in the legend, for different values of the attenuation factor β. The parameter values are $\tau_0 = 2.89 \times 10^{-10}$ and $d_0 = 2.17$ nm.
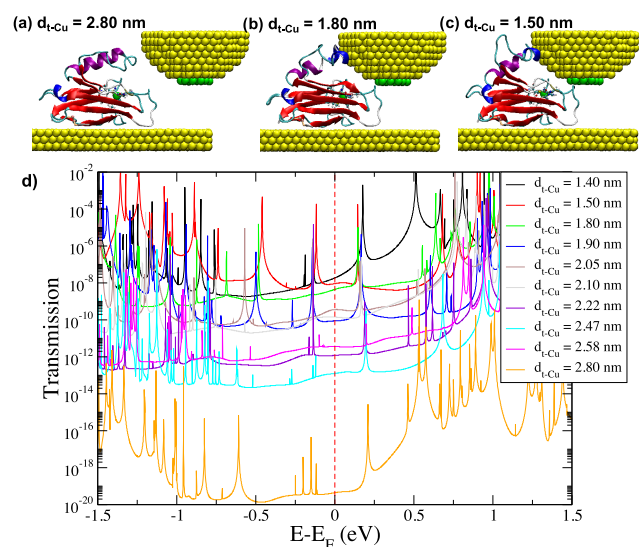

Figure 3. (a−c) Three representative junction geometries obtained during the MD simulations of the lateral indentation of the STM tip. The geometries are labeled according to the distance between the Cu atom in azurin and the central atom in the lowest tip layer, d_{t-Cu} (see more details in the SI). (d) Transmission as a function of energy for different geometries obtained in the lateral indentation simulations.

ref 37), which can be seen, globally, as an expansion of the overall structure. Nevertheless, it is worth noting that the electrical conductance of the blue-copper azurin measured by both blinking and break-junction techniques[18] showed actually low discrepancy in the results (conductance values between $10^{-6} G_0$ and $10^{-5} G_0$). We will come back to this issue further below.

DFT-Based Electron Transport Calculations. We choose to start our study by analyzing the conductive properties of the junctions obtained via the blinking method as their electronic structure was already analyzed in detail in ref 37. Figure 1a shows four representative geometries formed during the time trajectory; the transmission as a function of energy for the last three structures (subsequent to the formation of protein−gold contact) is shown in panels b−d of the same figure. Let us recall that within the Landauer formalism for coherent transport, the zero-bias conductance (at low temperatures) is determined by the transmission function, $\tau(E)$, evaluated at the Fermi energy, $E = E_F$, i.e., $G = G_0\tau(E_F)$. We observe that all transmission resonances are extremely narrow, indicating a very weak coupling of the corresponding orbitals with the metal leads. This is not surprising as all orbitals are highly localized in space.[36] Consequently, the conductance is extremely low. In Figure 1e, the transmission at the Fermi energy for the geometries obtained at 23 different MD time frames is reported. They fluctuate within the range of 10^{-16}−10^{-20}, which means that in practice the corresponding conductance values are many orders of magnitude below what is possible to measure in a single-protein junction (currently the highest current amplifications enable us to measure a conductance as low as 10^{-8}−$10^{-9} G_0$). The highest value observed at 200 ns stems from the highest occupied peak getting closer to the Fermi level than in the other frames. It is important to bear in mind that current DFT-based transport methods, like the one employed here, tend to overestimate the conductance values due to the well-known HOMO−LUMO gap inaccuracies in DFT with existing functionals.[76−78] Thus, the transmission values reported here can be considered as upper limits for the true values, which simply means that tunneling through these junction geometries is extremely unlikely. Notice also that, despite the structural fluctuations, the overall profile of the three transmission curves is rather similar. This is explained by the fact that, as already pointed out in ref 37, changes in the electronic structure through time mostly affect residues either involved in the metal−protein binding or located at the interface between the β-barrel and the α-helix.

Common wisdom suggests that the electron transport through blue-copper azurin takes place mainly through the Cu ion. To corroborate this, we have plotted the projected density of states on the Cu ion and compared its energy dependence with the corresponding transmission curve (see the SI). The comparison reveals that the Cu ion certainly plays an important role as it seems to contribute to the resonance closer to the Fermi energy in the occupied range. Nevertheless, the involvement of other residues (aspartic and glutamic acids, localized on the peripheral region of the protein) cannot be ruled out as they also contribute to states aligned at the same HOMO energy as the Cu ion (see the SI). Furthermore, we observe that, in panels c and d of Figure 1, the Fermi level is at an equal distance from the HOMO and LUMO peaks, which indicates that the involvement of the LUMO (localized on H35) should not be ruled out either.

We now turn to the analysis of the results obtained with the second contact approach described in the Introduction section, namely, from the simulation of the STM tip indentation (from the top). Figure 2a shows three representative geometries, corresponding to different tip−surface distances. The transmission values at the Fermi level obtained throughout the whole time trajectory as a function of such a distance are reported in panel d of the same figure. Despite fluctuations, it is possible to identify a clear trend, which indicates an exponential dependence with the tip−sample distance, with an attenuation factor of about 10−14 nm^{-1} (see the different dotted-dashed lines in panel d). These values for the attenuation factor are somewhat similar to those found in the analysis of the length dependence of the conductance in molecular junctions made of aromatic compounds and are clearly larger than those for conjugated molecules.[33]

The general shape of the transmission curves is similar to that obtained by the blinking process (see the SI). The transmission values achieved at the largest tip−surface distance are similar to those obtained in the blinking process. This is to be expected since in the blinking simulation the tip is kept at about the same distance from the surface (3.76 nm) as in the initial geometry used in the indentation process (3.79 nm). More importantly, at the smallest tip−surface distance, the transmission values are more than 6 orders of magnitude higher than the average value resulting from the blinking and, in some cases, those values are within the experimentally accessible range. This is particularly apparent in the geometry for a tip−surface distance of 2.54 nm in which the transmission at the Fermi energy is around 10^{-7}. As we show in the SI, this resonant behavior is due to the fact that the highest occupied orbital of the Cu ion lies in this case very close to the Fermi level of the junction. In general, the much higher transmission values in the indentation process are due to the reduction of the junction length due to the partial deformation of the protein and to an increase in the hybridization (or coupling) between the molecular states and metallic states of the leads.

Although the transmission values found in the indentation process are much higher than in the blinking, they still tend to be lower than that reported in single-protein STM-based experiments.[16,18] It has been hypothesized that the high conductance values reported in some of those experiments might be due to the fact that the protein is actually not contacted from the top but rather sideways. Naively, this would lead to junctions with a smaller effective length and, in turn, higher conductance values. To test this idea, we now turn to analyze the transmission as a function of energy for the geometries obtained by simulating a lateral indentation of the tip (Figure 3). In this example, we set the tip−surface distance to about 2 nm and move laterally the tip to contact the protein (see the SI for further details). As one can see in Figure 3d, all transmission resonances appear to be quite sharp as in the previous cases. As for the transmission at the Fermi level, the higher values are obviously obtained for the shorter protein−tip distance and are, in general, even higher than those obtained in the last steps of the top indentation. It can also be noticed that the LUMO-related peak is slightly broader than that corresponding to the HOMO, suggesting a better coupling to the leads and non-negligible contribution to the transport. Overall, these results suggest that the lateral indentation is a plausible scenario that could explain the observation of high conductance values in single-azurin experiments.

Influence of Water Molecules on the Electron Transport. To complete our systematic study, we would like to address an issue that is often debated, namely, the role in the electron transport of the water surrounding the junction but for which there is no rigorous theoretical analysis in the context of electron transport in protein junctions. Obviously, the presence of water affects the dynamics of the protein, and therefore, it is indirectly reflected in the transport properties via the geometry of the junction. However, it is by no means clear whether water molecules can alter the metal−protein coupling or even create direct pathways for the electron transport. The theoretical analysis of the role of water molecules on different types of systems has led to conflicting results in the literature. On the one hand, it has been suggested that water molecules can improve the electron-transfer rate in protein dimers[79−81] and can increase tunneling conductance by shifting molecular levels toward the Fermi energy[82] or introducing new levels at the lead−molecule interface.[83] On the other hand, the same were claimed to have a detrimental effect on the conductance by either reducing the metal−molecule coupling or modifying the level alignment.[84−87]

To resolve this issue in the context of metal−protein−metal junctions, we have performed some test calculations on our system by including some of the water molecules, which were initially present in the MD simulations. More specifically, we have included the first hydration layer (i.e., all water molecules within 3 Å from the protein), as depicted in Figure 4, and
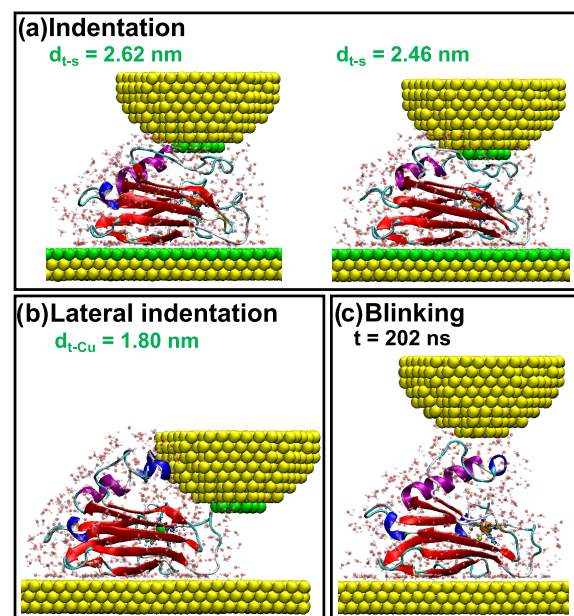

Figure 4. Junction geometries for which the role of the water molecules has been investigated: (a) tip indentation, (b) lateral indentation, and (c) blinking process.

consider examples for the three contact approaches or configurations discussed above. In particular, the results for the transmission curves for two geometries obtained in the top indentation, a geometry corresponding to the lateral indentation, and another one for the blinking process are shown in Figure 5. For each case, a comparison with the corresponding geometry in the absence of water is also shown. While no significant changes are observed for the two kinds of indentation, a conductance increase of around 2 orders of
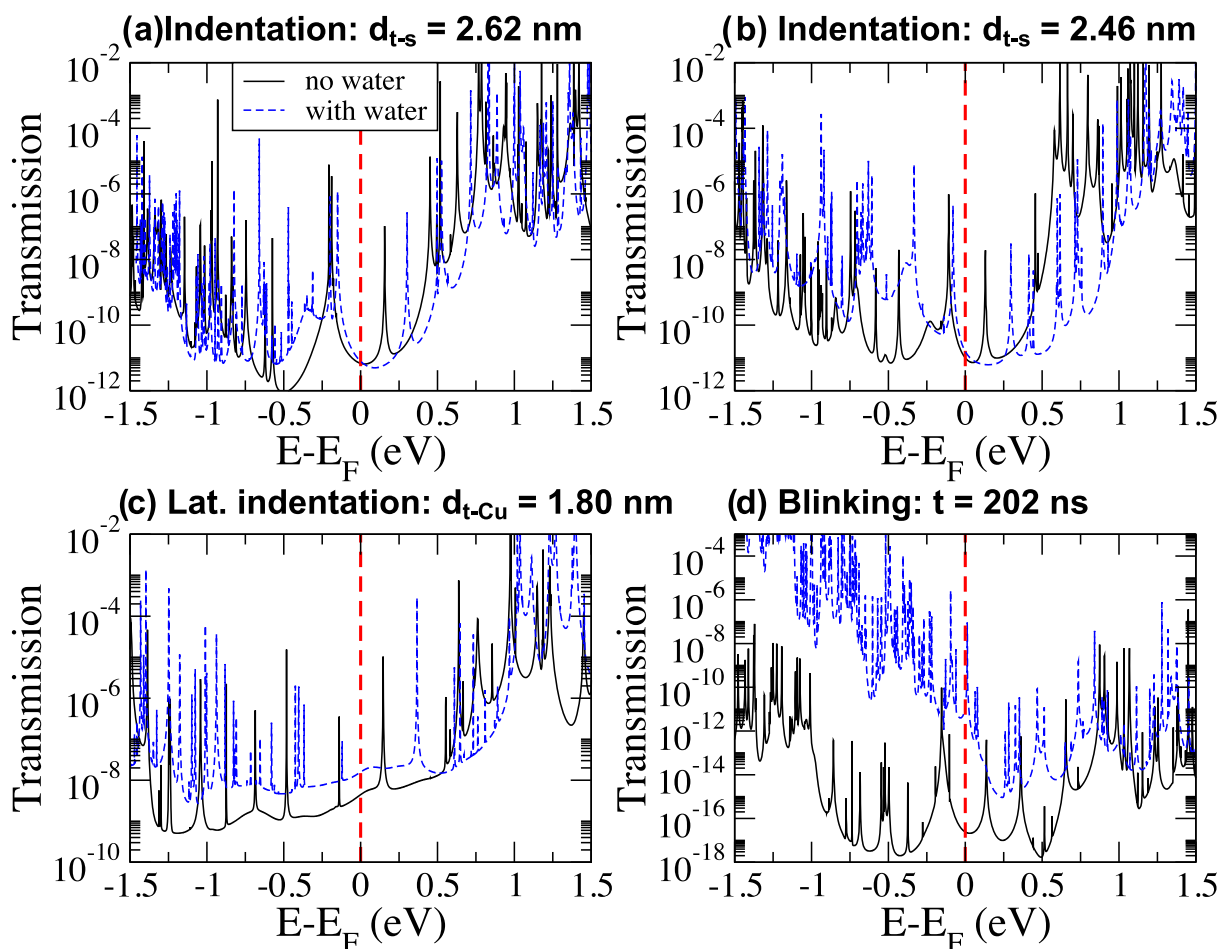
Figure 5. (a−d) Transmission as a function of energy for the four molecular junctions shown in Figure 4. The black solid lines correspond to the structures of Figure 4 deprived of the surrounding water molecules, whereas the blue dashed lines correspond to calculations in which the water molecules appearing in the same figure were explicitly taken into account. In all panels, the red dashed vertical lines indicate the position of the Fermi level.

magnitude is observed for the blinking. In the latter, an analysis of the projected density of states on each residue (not shown here) did not reveal a definitive global trend in the energy shift as the upward shift of some residue levels is compensated by the downward shifts of some others. Hence, energy shifts of molecular levels do not seem to be the origin of the conductance increase. Moreover, a calculation carried out on the same junction comprising only the water molecules (i.e., deprived of the protein) showed a transmission value at the Fermi level lower than 10^{-25}, indicating that they do not contribute to active channels for the conductance. Therefore, we ascribe the water-induced conductance increase observed in the blinking to an increase in the metal−protein coupling. Indeed, the transmission curve for the water-surrounded protein contains additional peaks with respect to the pristine case, in which, instead, they are too narrow to be shown with the energy resolution adopted in the calculation. This effect is probably more dramatic in the case of the blinking method than in the other cases because of the higher amount of water molecules included between the protein and tip.

■ CONCLUSIONS

In summary, we have studied the coherent component of the electron transport through junctions comprising a single blue-copper azurin from *P. aeruginosa*. Overall, our calculations strongly suggest that when the protein is gently contacted (from end to end), the tunneling probability is extremely small and the corresponding conductance is simply not measurable. However, we have also shown that a wide range of conductance values can be found, depending on the specific way the tip−protein contact is created, which in turn affects the metal−metal distance and the protein structural deformation. In particular, we have shown that scenarios like the lateral indentation can provide a plausible explanation for the strikingly high conductance values reported in some single-azurin STM experiments. We emphasize once more that in this work we focus on the analysis of the probability of coherent tunneling in azurin junctions and we have no claims or predictions about the efficiency of incoherent charge-transport mechanisms, whose rigorous analysis goes beyond the scope of this work. The methodology here employed allows us, in principle, to investigate whether the main conclusions drawn in this work also apply to other solid-state protein junctions, like, e.g., those based on cytochrome *c*.[13] Furthermore, it remains to be understood whether the coherent transport in junctions based on protein monolayers[15] is fundamentally different from that in the single-protein junctions discussed in this work.

ASSOCIATED CONTENT

ⓈI Supporting Information

The Supporting Information is available free of charge at https://pubs.acs.org/doi/10.1021/acs.jpcc.0c09364.

Details about the S–S bridge (Figure S1); electron transport calculations (Figures S2–S3); the lateral-indentation MD simulations (Figures S4–S5); the role of the Cu ion and projected density of states (Figures S6–S8); additional transmission curves (Figure S9); and the tip modeling in the lateral indentation (Figure S10) (PDF)

AUTHOR INFORMATION

Corresponding Authors

Juan Carlos Cuevas − *Departamento de Física Teórica de la Materia Condensada, Universidad Autónoma de Madrid, E-28049 Madrid, Spain; Condensed Matter Physics Center (IFIMAC), Universidad Autónoma de Madrid, E-28049 Madrid, Spain;* ⓞ orcid.org/0000-0001-7421-0682; Email: juancarlos.cuevas@uam.es

Linda A. Zotti − *Departamento de Física Teórica de la Materia Condensada, Universidad Autónoma de Madrid, E-28049 Madrid, Spain; Departamento de Física Aplicada I, Escuela Politécnica Superior, Universidad de Sevilla, Seville E-40011, Spain; Condensed Matter Physics Center (IFIMAC), Universidad Autónoma de Madrid, E-28049 Madrid, Spain;* ⓞ orcid.org/0000-0002-5292-6759; Email: lzotti@us.es

Authors

Carlos Romero-Muñiz − *Department of Physical, Chemical and Natural Systems, Universidad Pablo de Olavide, E-41013 Seville, Spain; Departamento de Física Teórica de la Materia Condensada, Universidad Autónoma de Madrid, E-28049 Madrid, Spain;* ⓞ orcid.org/0000-0001-6902-1553

María Ortega − *Departamento de Física Teórica de la Materia Condensada, Universidad Autónoma de Madrid, E-28049 Madrid, Spain*

J. G. Vilhena − *Department of Physics, University of Basel, CH-4056 Basel, Switzerland*

Ismael Díez-Pérez − *Department of Chemistry, Faculty of Natural & Mathematical Sciences, Kings College London, London SE1 1DB, U.K.;* ⓞ orcid.org/0000-0003-0513-8888

Rubén Pérez − *Departamento de Física Teórica de la Materia Condensada, Universidad Autónoma de Madrid, E-28049 Madrid, Spain; Condensed Matter Physics Center (IFIMAC), Universidad Autónoma de Madrid, E-28049 Madrid, Spain;* ⓞ orcid.org/0000-0001-5896-541X

Complete contact information is available at:
https://pubs.acs.org/10.1021/acs.jpcc.0c09364

Author Contributions

∇C. R.-M. and M. O. contributed equally to this work.

Notes

The authors declare no competing financial interest.

ACKNOWLEDGMENTS

REFERENCES

(1) Panda, S. S.; Katz, H. E.; Tovar, J. D. Solid-state Electrical Applications of Protein and Peptide Based Nanomaterials. *Chem. Soc. Rev.* **2018**, *47*, 3640−3658.

(2) Amdursky, N.; Marchak, D.; Sepunaru, L.; Pecht, I.; Sheves, M.; Cahen, D. Electronic Transport via Proteins. *Adv. Mater.* **2014**, *26*, 7142−7161.

(3) Eleonora, A.; Reggiani, L.; Pousset, J. *Sensors*; Springer, 2015; pp 3−7.

(4) Chi, Q.; Farver, O.; Ulstrup, J. Long-Range Protein Electron Transfer Observed at the Single-Molecule Level: In Situ Mapping of Redox-Gated Tunneling Resonance. *Proc. Natl. Acad. Sci. U.S.A.* **2005**, *102*, 16203−16208.

(5) Ortega, M.; Vilhena, J. G.; Zotti, L. A.; Díez-Pérez, I.; Cuevas, J. C.; Pérez, R. Tuning Structure and Dynamics of Blue Copper Azurin Junctions via Single Amino-Acid Mutations. *Biomolecules* **2019**, *9*, 611.

(6) Bostick, C. D.; Mukhopadhyay, S.; Pecht, I.; Sheves, M.; Cahen, D.; Lederman, D. Protein Bioelectronics: A Review of what We Do and Do not Know. *Rep. Prog. Phys.* **2018**, *81*, No. 026601.

(7) Ing, N. L.; El-Naggar, M. Y.; Hochbaum, A. I. Going the distance: long-range conductivity in protein and peptide bioelectronic materials. *J. Phys. Chem. B* **2018**, *122*, 10403−10423.

(8) Alessandrini, A.; Facci, P. Electron Transfer in Nanobiodevices. *Eur. Polym. J.* **2016**, *83*, 450−466.

(9) Ron, I.; Sepunaru, L.; Itzhakov, S.; Belenkova, T.; Friedman, N.; Pecht, I.; Sheves, M.; Cahen, D. Proteins as Electronic Materials: Electron Transport through Solid-State Protein Monolayer Junctions. *J. Am. Chem. Soc.* **2010**, *132*, 4131−4140.

(10) Sepunaru, L.; Pecht, I.; Sheves, M.; Cahen, D. Solid-State Electron Transport across Azurin: From a Temperature-Independent to a Temperature-Activated Mechanism. *J. Am. Chem. Soc.* **2011**, *133*, 2421−2423.

(11) Yu, X.; Lovrincic, R.; Sepunaru, L.; Li, W.; Vilan, A.; Pecht, I.; Sheves, M.; Cahen, D. Insights into Solid-State Electron Transport through Proteins from Inelastic Tunneling Spectroscopy: The Case of Azurin. *ACS Nano* **2015**, *9*, 9955−9963.

(12) Fereiro, J. A.; Porat, G.; Bendikov, T.; Pecht, I.; Sheves, M.; Cahen, D. Protein Electronics: Chemical Modulation of Contacts Control Energy Level Alignment in Gold-Azurin-Gold Junctions. *J. Am. Chem. Soc.* **2018**, *140*, 13317−13326.

(13) Fereiro, J. A.; Kayser, B.; Romero-Muñiz, C.; Vilan, A.; Dolgikh, D. A.; Chertkova, R. V.; Cuevas, J. C.; Zotti, L. A.; Pecht, I.; Sheves, M.; Cahen, D. A Solid-State Protein Junction Serves as a Bias-Induced Current Switch. *Angew. Chem., Int. Ed.* **2019**, *58*, 11852−11859.

(14) Kumar, K. S.; Pasula, R. R.; Lim, S.; Nijhuis, C. A. Long-Range Tunneling Processes across Ferritin-Based Junctions. *Adv. Mater.* **2016**, *28*, 1824−1830.

(15) Mukhopadhyay, S.; Karuppannan, S. K.; Guo, C.; Fereiro, J. A.; Bergren, A.; Mukundan, V.; Qiu, X.; Castañeda Ocampo, O. E.; Chen, X.; Chiechi, R. C.; et al. Solid-State Protein Junctions: Cross-Laboratory Study Shows Preservation of Mechanism at Varying Electronic Coupling. *iScience* **2020**, *23*, No. 101099.

(16) Artés, J. M.; Díez-Pérez, I.; Gorostiza, P. Transistor-like Behavior of Single Metalloprotein Junctions. *Nano Lett.* **2012**, *12*, 2679−2684.

(17) Artés, J. M.; López-Martínez, M.; Díez-Pérez, I.; Sanz, F.; Gorostiza, P. Conductance Switching in Single Wired Redox Proteins. *Small* **2014**, *10*, 2537−2541.

(18) Ruiz, M. P.; Aragonès, A. C.; Camarero, N.; Vilhena, J. G.; Ortega, M.; Zotti, L. A.; Pérez, R.; Cuevas, J. C.; Gorostiza, P.; Díez-Pérez, I. Bioengineering a Single-Protein Junction. *J. Am. Chem. Soc.* **2017**, *139*, 15337−15346.

(19) Li, W.; Sepunaru, L.; Amdursky, N.; Cohen, S. R.; Pecht, I.; Sheves, M.; Cahen, D. Temperature and Force Dependence of Nanoscale Electron Transport via the Cu Protein Azurin. *ACS Nano* **2012**, *6*, 10816−10824.

(20) Baldacchini, C.; Bizzarri, A. R.; Cannistraro, S. Electron Transfer, Conduction and Biorecognition Properties of the Redox Metalloprotein Azurin Assembled onto Inorganic Substrates. *Eur. Polym. J.* **2016**, *83*, 407−427.

(21) Kayser, B.; Fereiro, J. A.; Bhattacharyya, R.; Cohen, S. R.; Vilan, A.; Pecht, I.; Sheves, M.; Cahen, D. Solid-State Electron Transport via the Protein Azurin is Temperature-Independent Down to 4 K. *J. Phys. Chem. Lett.* **2020**, *11*, 144−151.

(22) Zhao, J.; Davis, J. J.; Sansom, M. S. P.; Hung, A. Exploring the Electronic and Mechanical Properties of Protein Using Conducting Atomic Force Microscopy. *J. Am. Chem. Soc.* **2004**, *126*, 5601−5609.

(23) Mukhopadhyay, S.; Dutta, S.; Pecht, I.; Sheves, M.; Cahen, D. Conjugated Cofactor Enables Efficient Temperature-Independent Electronic Transport across 6 nm Long Halorhodopsin. *J. Am. Chem. Soc.* **2015**, *137*, 11226−11229.

(24) Castañeda Ocampo, O. E.; Gordiichuk, P.; Catarci, S.; Gautier, D. A.; Herrmann, A.; Chiechi, R. C. Mechanism of Orientation-Dependent Asymmetric Charge Transport in Tunneling Junctions Comprising Photosystem I. *J. Am. Chem. Soc.* **2015**, *137*, 8419−8427.

(25) Garg, K.; Ghosh, M.; Eliash, T.; van Wonderen, J. H.; Butt, J. N.; Shi, L.; Jiang, X.; Zdenek, F.; Blumberger, J.; Pecht, I.; et al. Direct Evidence for Heme-Assisted Solid-State Electronic Conduction in Multi-Heme c-Type Cytochromes. *Chem. Sci.* **2018**, *9*, 7304−7310.

(26) Garg, K.; Raichlin, S.; Bendikov, T.; Pecht, I.; Sheves, M.; Cahen, D. Interface Electrostatics Dictates the Electron Transport via Bioelectronic Junctions. *ACS Appl. Mater. Interfaces* **2018**, *10*, 41599−41607.

(27) Fereiro, J. A.; Yu, X.; Pecht, I.; Sheves, M.; Cuevas, J. C.; Cahen, D. Tunneling Explains Efficient Electron Transport via Protein Junctions. *Proc. Natl. Acad. Sci. U.S.A.* **2018**, *115*, E4577.

(28) Migliore, A.; Nitzan, A. Nonlinear Charge Transport in Redox Molecular Junctions: A Marcus Perspective. *ACS Nano* **2011**, *5*, 6669−6685.

(29) Valianti, S.; Cuevas, J.-C.; Skourtis, S. S. Charge-Transport Mechanisms in Azurin-Based Monolayer Junctions. *J. Phys. Chem. C* **2019**, *123*, 5907−5922.

(30) Skourtis, S. S.; Waldeck, D. H.; Beratan, D. N. Fluctuations in Biological and Bioinspired Electron-Transfer Reactions. *Annu. Rev. Phys. Chem.* **2010**, *61*, 461−485.

(31) Stuchebrukhov, A. A. Long-Distance Electron Tunneling in Proteins. *Theor. Chem. Acc.* **2003**, *110*, 291−306.

(32) Hayashi, T.; Stuchebrukhov, A. A. Electron Tunneling in Respiratory Complex I. *Proc. Natl. Acad. Sci. U.S.A.* **2010**, *107*, 19157−19162.

(33) Cuevas, J. C.; Scheer, E. *Molecular Electronics: An Introduction to Theory and Experiment*, 2nd ed.; World Scientific, 2017.

(34) Kuznetsov, A. M.; Ulstrup, J. *Electron Transfer in Chemistry and Biology: An Introduction to the Theory*; John Wiley & Sons Ltd, 1999.

(35) Blumberger, J. Recent Advances in the Theory and Molecular Simulation of Biological Electron Transfer Reactions. *Chem. Rev.* **2015**, *115*, 11191−11238.

(36) Romero-Muñiz, C.; Ortega, M.; Vilhena, J. G.; Díez-Pérez, I.; Cuevas, J. C.; Pérez, R.; Zotti, L. A. Ab Initio Electronic Structure Calculations of Entire Blue Copper Azurins. *Phys. Chem. Chem. Phys.* **2018**, *20*, 30392−30402.

(37) Romero-Muñiz, C.; Ortega, M.; Vilhena, J. G.; Díez-Pérez, I.; Cuevas, J. C.; Pérez, R.; Zotti, L. A. Mechanical Deformation and Electronic Structure of a Blue Copper Azurin in a Solid-State Junction. *Biomolecules* **2019**, *9*, 506.

(38) Solomon, E. I.; Szilagyi, R. K.; DeBeer George, S.; Basumallick, L. Electronic Structures of Metal Sites in Proteins and Models: Contributions to Function in Blue Copper Proteins. *Chem. Rev.* **2004**, *104*, 419−458.

(39) Marshall, N. M.; Garner, D. K.; Wilson, T. D.; Gao, Y.-G.; Robinson, H.; Nilges, M. J.; Lu, Y. Rationally tuning the reduction potential of a single cupredoxin beyond the natural range. *Nature* **2009**, *462*, 113.

(40) Lancaster, K. M.; Zaballa, M.-E.; Sproules, S.; Sundararajan, M.; DeBeer, S.; Richards, J. H.; Vila, A. J.; Neese, F.; Gray, H. B. Outer-Sphere Contributions to the Electronic Structure of Type Zero Copper Proteins. *J. Am. Chem. Soc.* **2012**, *134*, 8241−8253.

(41) Lancaster, K. M.; Farver, O.; Wherland, S.; Crane, E. J., III; Richards, J. H.; Pecht, I.; Gray, H. B. Electron Transfer Reactivity of Type Zero *Pseudomonas aeruginosa* Azurin. *J. Am. Chem. Soc.* **2011**, *133*, 4865−4873.

(42) Farver, O.; Marshall, N. M.; Wherland, S.; Lu, Y.; Pecht, I. Designed Azurins Show Lower Reorganization Free Energies for Intraprotein Electron Transfer. *Proc. Natl. Acad. Sci. U.S.A.* **2013**, *110*, 10536−10540.

(43) Corni, S.; Rienzo, F. D.; Felice, R. D.; Molinari, E. Role of the Electronic Properties of Azurin Active Site in the Electron-Transfer Process. *Int. J. Quantum Chem.* **2005**, *102*, 328−342.

(44) Di Bilio, A. J.; Hill, M. G.; Bonander, N.; Karlsson, B. G.; Villahermosa, R. M.; Malmström, B. G.; Winkler, J. R.; Gray, H. B. Reorganization Energy of Blue Copper: Effects of Temperature and Driving Force on the Rates of Electron Transfer in Ruthenium- and Osmium-Modified azurins. *J. Am. Chem. Soc.* **1997**, *119*, 9921−9922.

(45) Carey, R.; Chen, L.; Gu, B.; Franco, I. When Can Time-Dependent Currents Be Reproduced by the Landauer Steady-State Approximation? *J. Chem. Phys.* **2017**, *146*, No. 174101.

(46) Popescu, B.; Woiczikowski, P. B.; Elstner, M.; Kleinekathöfer, U. Time-Dependent View of Sequential Transport through Molecules with Rapidly Fluctuating Bridges. *Phys. Rev. Lett.* **2012**, *109*, No. 176802.

(47) Haiss, W.; Nichols, R. J.; van Zalinge, H.; Higgins, S. J.; Bethell, D.; Schiffrin, D. J. Measurement of Single Molecule Conductivity Using the Spontaneous Formation of Molecular Wires. *Phys. Chem. Chem. Phys.* **2004**, *6*, 4330−4337.

(48) Haiss, W.; Wang, C.; Grace, I.; Batsanov, A. S.; Schiffrin, D. J.; Higgins, S. J.; Bryce, M. R.; Lambert, C. J.; Nichols, R. J. Precision Control of Single-Molecule Electrical Junctions. *Nat. Mater.* **2006**, *5*, 995−1002.

(49) Díez-Pérez, I.; Hihath, J.; Lee, Y.; Yu, L.; Adamska, L.; Kozhushner, M. A.; Oleynik, I. I.; Tao, N. Rectification and Stability of a Single Molecular Diode with Controlled Orientation. *Nat. Chem.* **2009**, *1*, 635.

(50) Aragonès, A. C.; Darwish, N.; Ciampi, S.; Sanz, F.; Gooding, J. J.; Díez-Pérez, I. Single-Molecule Electrical Contacts on Silicon Electrodes under Ambient Conditions. *Nat. Commun.* **2017**, *8*, No. 15056.

(51) Case, D. A.; Darden, T. A.; T, E. C.; Simmerling, C.; Wang, J.; Duke, R.; Luo, R.; Walker, R.; Zhang, W.; Merz, K. et al. *AMBER 14*; University of California, San Francisco, 2014. http://ambermd.org/.

(52) Salomon-Ferrer, R.; Götz, A. W.; Poole, D.; Le Grand, S.; Walker, R. C. Routine Microsecond Molecular Dynamics Simulations with AMBER on GPUs. 2. Explicit Solvent Particle Mesh Ewald. *J. Chem. Theory Comput.* **2013**, *9*, 3878−3888.

(53) Götz, A. W.; Williamson, M. J.; Xu, D.; Poole, D.; LeGrand, S.; Walker, R. C. Routine Microsecond Molecular Dynamics Simulations with AMBER on GPUs. 1. Generalized Born. *J. Chem. Theory Comput.* **2012**, *8*, 1542−1555.

(54) Grand, S. L.; Götz, A. W.; Walker, R. C. SPFP: Speed without Compromise: A Mixed Precision Model for GPU Accelerated

Molecular Dynamics Simulations. *Comput. Phys. Commun.* **2013**, *184*, 374–380.

(55) Maier, J. A.; Martinez, C.; Kasavajhala, K.; Wickstrom, L.; Hauser, K. E.; Simmerling, C. ff14SB: Improving the Accuracy of Protein Side Chain and Backbone Parameters from ff99SB. *J. Chem. Theory Comput.* **2015**, *11*, 3696–3713.

(56) van den Bosch, M.; Swart, M.; Snijders, J. G.; Berendsen, H. J. C.; Mark, A. E.; Oostenbrink, C.; van Gunsteren, W. F.; Canters, G. W. Calculation of the Redox Potential of the Protein Azurin and Some Mutants. *ChemBioChem* **2005**, *6*, 738–746.

(57) Paltrinieri, L.; Borsari, M.; Ranieri, A.; Battistuzzi, G.; Corni, S.; Bortolotti, C. A. The Active Site Loop Modulates the Reorganization Energy of Blue Copper Proteins by Controlling the Dynamic Interplay with Solvent. *J. Phys. Chem. Lett.* **2013**, *4*, 710–715.

(58) Beedle, A. E. M.; Lezamiz, A.; Stirnemann, G.; Garcia-Manyes, S. The Mechanochemistry of Copper Reports on the Directionality of Unfolding in Model Cupredoxin Proteins. *Nat. Commun.* **2015**, *6*, No. 7894.

(59) Zanetti-Polzi, L.; Bortolotti, C. A.; Daidone, I.; Aschi, M.; Amadei, A.; Corni, S. A Few Key Residues Determine the High Redox Potential Shift in Azurin Mutants. *Org. Biomol. Chem.* **2015**, *13*, 11003–11013.

(60) Zanetti-Polzi, L.; Corni, S.; Daidone, I.; Amadei, A. Extending the Essential Dynamics Analysis to Investigate Molecular Properties: Application to the Redox Potential of Proteins. *Phys. Chem. Chem. Phys.* **2016**, *18*, 18450–18459.

(61) Berman, H. M.; Westbrook, J.; Feng, Z.; Gilliland, G.; Bhat, T. N.; Weissig, H.; Shindyalov, I. N.; Bourne, P. E. The Protein Data Bank. *Nucleic Acids Res.* **2000**, *28*, 235–242.

(62) Nar, H.; Messerschmidt, A.; Huber, R.; van de Kamp, M.; Canters, G. W. Crystal Structure Analysis of Oxidized *Pseudomonas aeruginosa* Azurin at pH 5.5 and pH 9.0: A pH-Induced Conformational Transition Involves a Peptide Bond Flip. *J. Mol. Biol.* **1991**, *221*, 765–772.

(63) Gordon, J. C.; Myers, J. B.; Folta, T.; Shoja, V.; Heath, L. S.; Onufriev, A. H++: a Server for Estimating pKas and Adding Missing Hydrogens to Macromolecules. *Nucleic Acids Res.* **2005**, *33*, W368–W371.

(64) Heinz, H.; Lin, T.-J.; Kishore Mishra, R.; Emami, F. S. Thermodynamically Consistent Force Fields for the Assembly of Inorganic, Organic, and Biological Nanostructures: The INTERFACE Force Field. *Langmuir* **2013**, *29*, 1754–1765.

(65) Heinz, H.; Ramezani-Dakhel, H. Simulations of Inorganic-Bioorganic Interfaces to Discover New Materials: Insights, Comparisons to Experiment, Challenges, and Opportunities. *Chem. Soc. Rev.* **2016**, *45*, 412–448.

(66) Pawlak, R.; Vilhena, J. G.; Hinaut, A.; Meier, T.; Glatzel, T.; Baratoff, A.; Gnecco, E.; Pérez, R.; Meyer, E. Conformations and Cryo-Force Spectroscopy of Spray-Deposited Single-Strand DNA on Gold. *Nat. Commun.* **2019**, *10*, No. 685.

(67) Scherb, S.; Hinaut, A.; Pawlak, R.; Vilhena, J. G.; Liu, Y.; Freund, S.; Liu, Z.; Feng, X.; Müllen, K.; Glatzel, T.; Narita, A.; Meyer, E. Giant Thermal Expansion of a Two-Dimensional Supramolecular Network Triggered by Alkyl Chain Motion. *Commun. Mater.* **2020**, *1*, 8.

(68) Jorgensen, W. L.; Chandrasekhar, J.; Madura, J. D.; Impey, R. W.; Klein, M. L. Comparison of Simple Potential Functions for Simulating Liquid Water. *J. Chem. Phys.* **1983**, *79*, 926–935.

(69) Ozaki, T. Variationally Optimized Atomic Orbitals for Large-Scale Electronic Structures. *Phys. Rev. B* **2003**, *67*, No. 155108.

(70) Ozaki, T.; Kino, H. Numerical Atomic Basis Orbitals from H to Kr. *Phys. Rev. B* **2004**, *69*, No. 195113.

(71) Perdew, J. P.; Burke, K.; Ernzerhof, M. Generalized Gradient Approximation Made Simple. *Phys. Rev. Lett.* **1996**, *77*, 3865.

(72) Morrison, I.; Bylander, D. M.; Kleinman, L. Nonlocal Hermitian Norm-Conserving Vanderbilt Pseudopotential. *Phys. Rev. B* **1993**, *47*, 6728.

(73) Zotti, L. A.; Pérez, R. Platinum Atomic Contacts: From Tunneling to Contact. *Phys. Rev. B* **2017**, *95*, No. 125438.

(74) Kresse, G.; Furthmüller, J. Efficient Iterative Schemes for Ab Initio Total-Energy Calculations Using a Plane-Wave Basis Set. *Phys. Rev. B* **1996**, *54*, 11169–11186.

(75) Kerker, G. P. Efficient Iteration Scheme for Self-Consistent Pseudopotential Calculations. *Phys. Rev. B* **1981**, *23*, 3082–3084.

(76) Jakobsen, S.; Kristensen, K.; Jensen, F. Electrostatic Potential of Insulin: Exploring the Limitations of Density Functional Theory and Force Field Methods. *J. Chem. Theory Comput.* **2013**, *9*, 3978–3985.

(77) Zhao, Q.; Kulik, H. J. Where Does the Density Localize in the Solid State? divergent behavior for hybrids and DFT+ U. *J. Chem. Theory Comput.* **2018**, *14*, 670–683.

(78) Bao, J. L.; Gagliardi, L.; Truhlar, D. G. Self-Interaction Error in Density Functional Theory: An Appraisal. *J. Phys. Chem. Lett.* **2018**, *9*, 2353–2358.

(79) Migliore, A.; Corni, S.; Di Felice, R.; Molinari, E. Water-Mediated Electron Transfer between Protein Redox Centers. *J. Phys. Chem. B* **2007**, *111*, 3774–3781.

(80) Lin, J.; Balabin, I. A.; Beratan, D. N. The Nature of Aqueous Tunneling Pathways between Electron-Transfer Proteins. *Science* **2005**, *310*, 1311–1313.

(81) Cárdenas, D. J.; Cuerva, J. M.; Alías, M.; Buñuel, E.; Campaña, A. G. Water-Based Hydrogen-Atom Wires as Mediators in Long-Range Proton-Coupled Electron Transfer in Enzymes: A New Twist on Water Reactivity. *Chem. - Eur. J.* **2011**, *17*, 8318–8323.

(82) Leary, E.; Höbenreich, H.; Higgins, S. J.; van Zalinge, H.; Haiss, W.; Nichols, R. J.; Finch, C. M.; Grace, I.; Lambert, C. J.; McGrath, R.; Smerdon, J. Single-Molecule Solvation-Shell Sensing. *Phys. Rev. Lett.* **2009**, *102*, No. 086801.

(83) Clément, N.; Guerin, D.; Pleutin, S.; Godey, S.; Vuillaume, D. Role of Hydration on the Electronic Transport through Molecular Junctions on Silicon. *J. Phys. Chem. C* **2012**, *116*, 17753–17763.

(84) Zotti, L. A.; Bednarz, B.; Hurtado-Gallego, J.; Cabosart, D.; Rubio-Bollinger, G.; Agrait, N.; van der Zant, H. S. J. Can One Define the Conductance of Amino Acids? *Biomolecules* **2019**, *9*, 580.

(85) Atesci, H.; Kaliginedi, V.; Gil, J. A. C.; Ozawa, H.; Thijssen, J. M.; Broekmann, P.; Haga, M.-a.; van der Molen, S. J. Humidity-Controlled Rectification Switching in Ruthenium-Complex Molecular Junctions. *Nat. Nanotechnol.* **2018**, *13*, 117–121.

(86) Long, D. P.; Lazorcik, J. L.; Mantooth, B. A.; Moore, M. H.; Ratner, M. A.; Troisi, A.; Yao, Y.; Ciszek, J. W.; Tour, J. M.; Shashidhar, R. Effects of Hydration on Molecular Junction Transport. *Nat. Mater.* **2006**, *5*, 901–908.

(87) Ai, Y.; Kovalchuk, A.; Qiu, X.; Zhang, Y.; Kumar, S.; Wang, X.; Kühnel, M.; Nørgaard, K.; Chiechi, R. C. In-Place Modulation of Rectification in Tunneling Junctions Comprising Self-Assembled Monolayers. *Nano Lett.* **2018**, *18*, 7552–7559.